Available online at www.sciencedirect.com
SCIENCE DIRECT®
Journal of Nuclear Materials 350 (2006) 293–300
journal of nuclear materials
www.elsevier.com/locate/jnucmat

Recrystallisation of amorphous natural brannerite through annealing: The effect of radiation damage on the chemical durability of brannerite

Y. Zhang [a,*], G.R. Lumpkin [b], H. Li [a], M.G. Blackford [a,b], M. Colella [a], M.L. Carter [a], E.R. Vance [a]

[a] Australian Nuclear Science and Technology Organisation, PMB 1, Menai, NSW 2234, Australia
[b] Department of Earth Sciences, University of Cambridge, Downing Street, Cambridge CB2 3EQ, UK

Received 25 May 2005; accepted 3 January 2006

Abstract

An amorphous natural brannerite sample was chosen to study the annealing of the radiation damage through thermal recrystallisation, and subsequently to evaluate the effect of radiation damage on its aqueous durability. Microstructural characterisation of the natural brannerite revealed minor alteration along the rim of the crystal and within cracks. The formation of UO_2 particles and soluble Pb–Ca-rich aluminosilicate glass is responsible for the higher U and Pb releases from the recrystallised brannerite. In general, natural brannerite has been shown to be resistant to dissolution over geological time, therefore minor brannerite inclusions in ceramic formulations for immobilisation of actinide-rich radioactive wastes should not have a detrimental effect on the long-term chemical durability of the wasteforms.

1. Introduction

In nature, brannerite has been characterised as a resistant mineral with the general formula $U_{1-x}Ti_{2+x}O_6$ [1,2]. It is one of the few ore minerals of uranium and is also notable as a heavy mineral in all vial sediments, having been concentrated through weathering of the host rock. Its crystal structure is monoclinic and both the U and Ti atoms are in distorted octahedral coordination [3]. Natural brannerite generally contains impurity elements including Pb, Ca, Th, Y and REE on the U-site, and Si, Al and Fe on the Ti-site [4]. It is normally amorphous due to alpha-decay damage given its geological age and high U content [4]. The presence of Pb is mainly due to the decay of U and Th (e.g., ^{238}U and ^{232}Th series).

Brannerite also exists, as a minor phase, in the ceramic formulations designed for the immobilisation of surplus Pu [5]. The crystal chemistry, radiation effects and aqueous dissolution of brannerite have been recently studied in detail [6,7]. It is of interest to understand better the effect of radiation

* Corresponding author. Tel.: +61 2 9717 9156; fax: +61 2 9543 7179.
E-mail address: yzx@ansto.gov.au (Y. Zhang).

0022-3115/$ - see front matter © 2006 Elsevier B.V. All rights reserved.
doi:10.1016/j.jnucmat.2006.01.012

damage on its chemical stability through the recrystallisation process of amorphous natural brannerite on annealing. The recrystallisation of natural amorphous brannerite on annealing at ~1000 °C has been confirmed by X-ray diffraction (XRD) [6,8], thermogravitry/differential thermal analysis (TG/DTA) [6,9] and emanation thermal analysis (ETA) [9]. However, no detailed microscopic characterisation on the recrystallisation of natural brannerite has been reported. In the present study, an amorphous natural brannerite from southern Spain was used as an example to study the details of its thermal recrystallisation and the effect of radiation damage on its chemical durability.

2. Experimental

2.1. Samples and methods

The natural brannerite sample used in this study is from the El Cabril mine, near Cordoba, in the Sierra Albarrana region of southern Spain. The host rock for this brannerite is a granitic pegmatite, located within 400–600 Ma metasedimentary and igneous rocks of the region. The Th–U–Pb chemical age of this sample, calculated from an average SEM-EDX analysis [10], is 476 Ma, in good agreement with the known ages of the host rocks. Brannerite from the Sierra Albarrana region is typically associated with feldspars, quartz, muscovite, apatite, beryl, and garnet, among other pegmatite minerals.

The sample was annealed in argon atmosphere at 500, 700, 900 and 1100 °C for 1 h. The annealed samples were then crushed to 75–150 μm and washed with acetone to remove the fine particles on the surface. Surface areas measured by BET method are summarised in Table 1. The powdered samples were examined by X-ray diffraction (XRD), SEM, TEM and subsequently by aqueous leaching.

Table 1
BET surface areas for the natural brannerite samples annealed at different temperatures

	Un-heated	500 °C	700 °C	900 °C	1100 °C
BET surface area (m^2/g)	0.33	0.74	0.38	0.23	0.12
Pore volume (cm^3/g)	0.0012	0.0016	0.0021	0.0018	0.0005
BET pore diameter (nm)	14.0	7.7	14.5	7.4	5.7

Batch leaching tests were carried out using a pH 4 solution (0.01 M KH_2phthalate adjusted with 1 M HNO_3) in polystyrene containers within an oven at 30 °C. The initial solid concentration was ~0.02 g in 30 mL solution. Aliquots (2 mL) were regularly taken, run through 0.25 μm filters, and then acidified with 3% by volume of analytical grade HNO_3. An inductively coupled plasma mass spectrometer (ICP-MS) was used to determine the elemental concentrations in the solutions.

2.2. Scanning electron microscopy (SEM)

Secondary and backscattered electron images, together with detailed microanalyses, were obtained using a JEOL 6400 SEM equipped with a Noran Voyager EDX system. All observations were made using a polished section of the natural brannerite. Images were acquired on Polaroid image film using an operating voltage of 15 kV. Microanalyses were acquired for 500 s live time using an operating voltage of 25 kV (dead time was 30–35%) and processed with the Noran software set up for standardless mode. In this mode, the correction parameters were optimised using a large collection of minerals and synthetic compounds. Spectra were processed using a digital top-hat filter for background correction, a multiple least squares fitting procedure for determination of peak counts, and full ZAF matrix correction.

2.3. Transmission electron microscopy (TEM)

Diffraction patterns, bright field images, and microanalyses were obtained at using a JEOL 2000fxII operated at 200 kV and equipped with a complete Link ISIS EDX system. For this work, we used crushed grains of the brannerite dispersed onto holey carbon grids. Electron diffraction work was carried out using a nominal camera length of 80 cm. For accurate measurement of *d*-spacings, the instrument has been calibrated at this camera length for a range of objective lens current settings using a gold standard. EDX analyses were generally acquired for 300 s and processed using a digital top-hat filter to remove the background. A multiple least squares fitting routine was employed to determine the peak counts, using a set of experimental *k*-factors determined from a large suite of silicate and oxide reference materials [11].

3. Results and discussion

3.1. Characterisation of unheated sample by SEM

Secondary and backscattered electron images demonstrate that the brannerite specimen is largely unaltered, with the exception of a zone along the rim of the crystal that is approximately 50–500 μm wide (Fig. 1). Some alteration also occurs along fractures extending well into the sample. These alteration zones are generally much narrower, ranging from a few micrometers up to a maximum of 50 μm across. The alteration is easily observed using backscattered electron imaging, revealed by darker contrast (lower mean atomic number). Images taken at higher magnification also revealed the presence of numerous inclusions of a phase with higher average atomic number, but these were too small (generally <1 μm) to identify by EDX analysis. The inclusions are not uniformly distributed throughout the sample, and some areas of the unaltered brannerite are essentially inclusion-free.

The chemical formula of the sample exhibits a total cation value significantly in excess of 3.00 per mole, indicating that higher levels of U^{5+} and/or U^{6+} are present. Furthermore, the sample has a deficit at the B-site and an excess of cations at the A-site, suggesting that Y and some of the U may occupy the B-site. The average formal U valence state of the sample is equal to 5.03 based on charge balance calculations. This value is in good agreement with the value of 4.80 determined by electron energy loss spectroscopy (EELS) [10] and diffuse reflectance spectroscopy showed an electronic absorption peak attributed to U^{5+} and peaks from U^{4+} [6].

3.2. Characterisation of unheated sample by TEM

Electron diffraction patterns obtained from grains of the unaltered brannerite, prior to the heat treatments, are dominated by the presence of diffuse rings with equivalent *d*-spacings of 0.31 and 0.19 nm. These spacings are typical of a range of titanate, niobate, and tantalate materials that are rendered amorphous by alpha-decay damage. Certain grains also exhibit weak diffraction spots that derive from numerous small inclusions apparent in bright field images and noted above in the SEM section. Measured *d*-spacings of these diffraction spots correspond to the strongest reflections of crystalline uraninite inclusions in the 10–100 nm size range (Fig. 2). A quantitative thin film EDX analysis of one of the inclusions showed about 91 wt% UO_2, about 5 wt% PbO, and minor amounts of Ca and Th.

We also examined several altered areas by electron diffraction and found that these areas remained amorphous or poorly crystalline, in spite of the observed chemical changes relative to the unaltered brannerite. Some of the grains showed very weak spotty rings, consistent with a localised, incipient stage of recrystallisation. Nevertheless, the TEM results are generally consistent with X-ray diffraction work that shows that the bulk of the sample is amorphous. This is due to the high U content

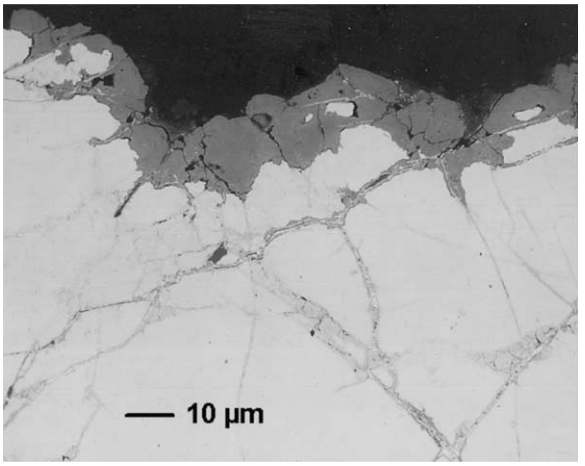

Fig. 1. Backscattered electron image of the natural brannerite indicated that the sample is largely free of alteration, except for a thin (~100 μm) alteration rind revealed by darker contrast in the image.

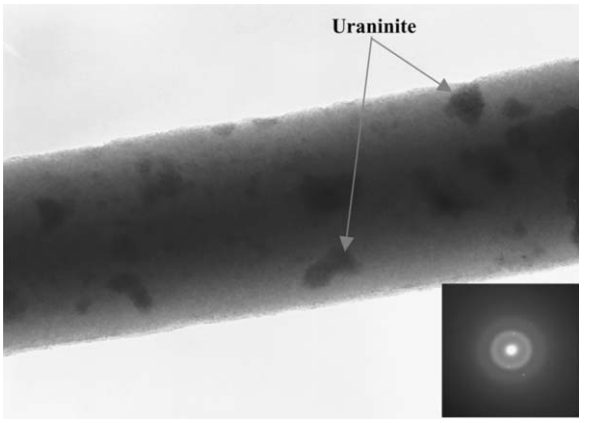

Fig. 2. TEM bright field image (width of the image is equal to 0.5 μm) demonstrates that the sample is essentially amorphous (metamict), but contains numerous uraninite crystalline inclusions in the 10–100 nm size range.

and great age of the sample, leading to a high cumulative alpha decay dose of approximately 6.9×10^{17} α/mg, well above the estimated critical amorphization dose of natural brannerite which is approximately $1–3 \times 10^{16}$ α/mg [10].

3.3. Characterisation of recrystallisation by XRD and SEM

XRD after annealing at 500, 700, 900, 1100 and 1300 °C suggested that the major recrystallisation took place between 900 and 1100 °C. The BET surface area decreases with increasing of the annealing temperature while the pore volume increases on heating at 500–700 °C and then decreases afterwards (see Table 1). The Archimedes' density decreases gradually from 5.0 (unheated) to 4.8 g cm^{-3} on heating at 500–900 °C, before increasing to 5.2 g cm^{-3} after heating at 1100 and 1300 °C [6]. The density pattern is broadly in agreement with the relatively higher pore volumes at 500–900 °C (see Table 1).

The average chemical compositions of relatively unaltered and altered areas are shown in Table 2 (assuming all U is U^{4+}). The altered areas have generally lost some amounts of UO_2, MgO, FeO and CaO, and to some extent have gained SiO_2, Y_2O_3, Ln_2O_3, P_2O_5 and As_2O_5. The average chemical compositions of relatively unaltered areas after annealing at 500, 700, 900 and 1100 °C are also included in Table 2. With increasing of annealing temperatures, CaO and PbO are gradually reduced in the unaltered areas, and SiO_2 is also reduced after 900 °C, suggesting mobility of these elements during the recrystallisation process.

Table 2
Average compositions of relatively unaltered and altered areas before and after annealing at different temperatures

	Altered	Unaltered	Unaltered			
	Unheated	Unheated	500 °C	700 °C	900 °C	1100 °C
SiO_2	3.0	0.3	0.3	0.6	0.2	0.1
TiO_2	38.6	34.7	33.2	34.3	35.7	38.7
ZrO_2	0.0	0.1	0.1	0.1	0.1	0.1
ThO_2	1.5	1.2	2.3	1.2	1.2	1.2
UO_2	43.6	54.3	53.5	53.9	54.1	53.3
Al_2O_3	0.7	0.8	0.7	0.7	0.7	0.7
Y_2O_3	1.3	0.3	0.3	0.3	0.3	0.2
MgO	0.0	0.2	0.7	0.7	0.5	0.2
CaO	3.0	3.9	4.0	3.8	3.7	3.0
MnO	0.3	0.2	0.4	0.3	0.5	0.2
FeO	1.2	1.5	1.7	1.4	1.7	1.4
Ln_2O_3	1.8	0.1	0.3	0.2	0.1	0.3
PbO	3.7	2.6	2.4	2.3	1.1	0.4
P_2O_5	0.1					
As_2O_5	1.1					

Based on five analyses of each sample.

3.4. Characterisation of recrystallisation by TEM

TEM bright field images and electron diffraction patterns of the heated samples are shown in Figs. 3–6. As shown in Fig. 3, the sample heated at 500 °C is amorphous and essentially unchanged with respect to the unheated starting material. The chemical composition of the sample, with the exception of the Th content, is also within error of that of the unheated sample (see Table 2). TEM examination of the sample heated at 700 °C demonstrates that the material has partially recrystallised. Fig. 4 illustrates the presence of both amorphous and polycrystalline grains in this sample. The crystalline material exhibits a grain size of approximately 5–40 nm, resulting in the characteristic ring type of diffraction pattern. Upon annealing at 900 °C, the amorphous material has fully recrystallised and the brannerite crystallites range from about 10 nm up to about 500 nm in size. The grain size and resulting electron diffraction patterns obtained at this annealing temperature are illustrated in Fig. 5. The composition of the recrystallised brannerite is close to that of the unheated sample, with the

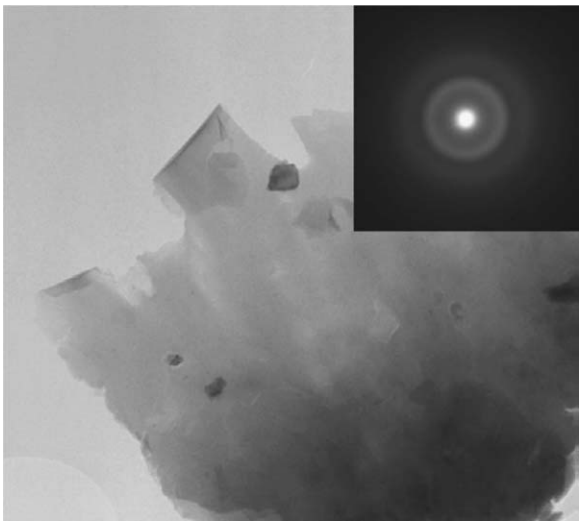

Fig. 3. TEM bright field image (width of the image is equal to 1.0 μm) and electron diffraction pattern of the sample heated at 500 °C. The sample remains amorphous at this temperature and is virtually identical to the unheated starting material. Small dark inclusions in the image are anatase crystals.

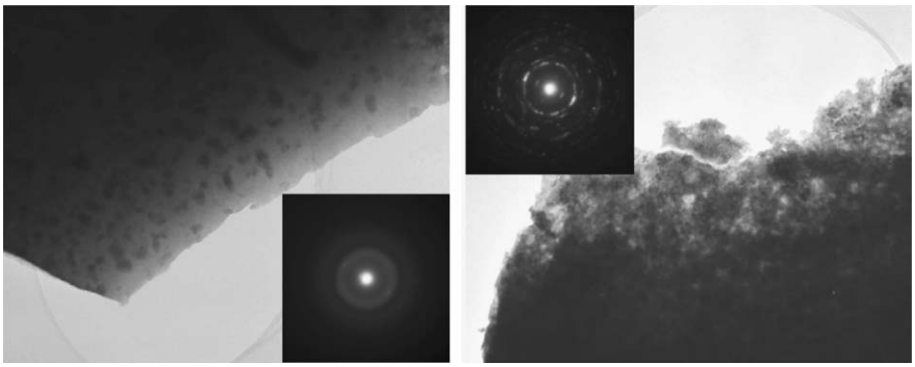

Fig. 4. TEM bright field images (width of each image is equal to 1.0 μm) and selected area diffraction patterns of brannerite annealed at 700 °C. Some grains are still amorphous, with inclusions of UO_2, as illustrated by the image and the diffraction pattern on the left. Many grains at this temperature have recrystallised to a polycrystalline aggregate, as shown by the image and the diffraction pattern on the right.

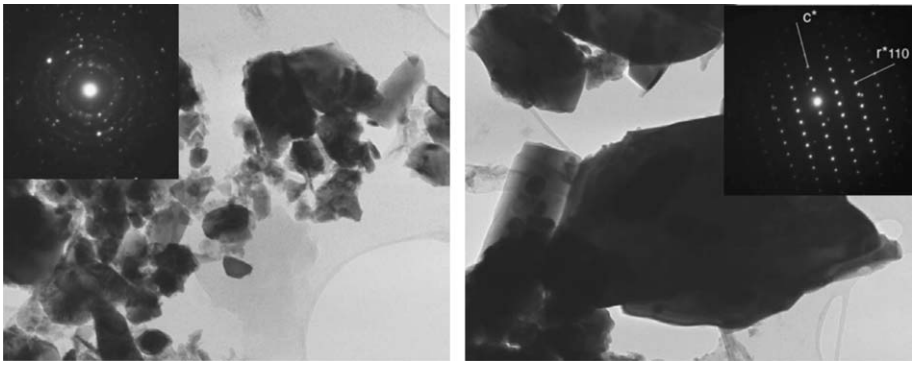

Fig. 5. TEM bright field images (width of each image is equal to 1.0 μm) and selected area diffraction patterns of brannerite annealed at 900 °C. These images illustrate the range in grain size and the absence of amorphous material after heating at this temperature.

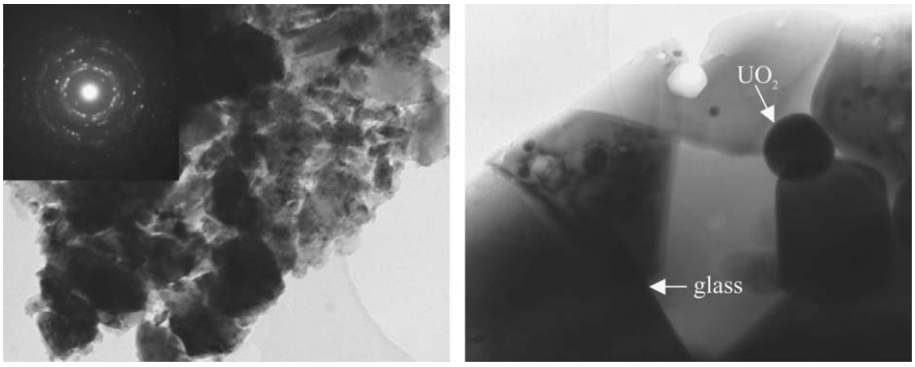

Fig. 6. TEM bright field images (width of the image is equal to 1.0 μm) and selected area diffraction pattern of brannerite annealed at 1100 °C. The image on the left shows that some relatively fine grained polycrystalline material persists at this temperature. Some large grains have recrystallised to an assemblage of brannerite + uraninite + glass, as shown by the image on the right.

exception of some Pb loss (Table 2). After heating at 1100 °C, the grain size has increased substantially, and is typically in the 40–2000 nm size range as shown in the TEM bright field images of Fig. 6. The TEM-EDX analysis reveals further Pb loss and some Ca loss from the crystalline brannerite at this temperature. Many of the large polycrystalline grains also exhibit 100–400 nm spheres of

Table 3
Analysis of glass phase observed by TEM in the sample annealed at 1100 °C

Oxide	Wt (%)	Oxide	Wt (%)
P_2O_5	1.2	Al_2O_3	16.6
As_2O_5	0.0	Y_2O_3	0.2
SiO_2	65.5	Ln_2O_3	0.1
TiO_2	1.6	MgO	1.0
ZrO_2	0.0	CaO	6.7
ThO_2	0.0	MnO	1.7
UO_2	0.9	FeO	1.0
Na_2O	0.2	PbO	3.3

uraninite and interstitial glass. The chemical microanalysis of the latter phase shows that it is a Ca-aluminosilicate type glass with significant amounts of Pb, Ti, Ca, Mn, Fe, and other minor elements (see Table 3).

The electron diffraction patterns (Fig. 4 right, Fig. 5 left and Fig. 6 left) each contain diffracted beams arising from numerous crystals with different grain sizes. The grains are, in most cases, too large to give really good ring patterns. Measured *d*-spacings are similar in all of the patterns and are consistent with the identification as brannerite. Some rutile may also be present, but the strongest diffracted beams, e.g., the (1 1 0) at 0.325 nm and the (0 1 1) at 0.249 nm, are very close to those of brannerite. Typical *d*-spacings and *hkl* indices are 0.61 nm (0 0 1), 0.35 nm (1 −1 0), 0.33 nm (−2 0 2), 0.29 nm (2 0 1), 0.27 nm (1 −1 1), 0.24 nm (−3 1 1).

The single crystal zone axis pattern (Fig. 5 right) contains the (0 0 1), (1 1 0), and (1 1 −1) diffracted beams at 0.61 nm, 0.35 nm, and 0.27 nm, respectively. The pattern was identified as the [−1 1 0] zone of brannerite on this basis and subsequently matched with a calculated diffraction pattern. We have indexed a selection of the diffracted beams on this pattern.

3.5. Chemical durability of the natural brannerite

Based on BET-determined surface areas, the elemental release rates ($g\,m^{-2}\,d^{-1}$) for the samples annealed at different temperatures are shown in Figs. 7–11. Generally they decrease slightly with time except for Th and Y after annealing at 700 °C. U and Ca have similar elemental release patterns with the highest release rates at 700–900 °C, following by those at 1100 °C and the lowest at 500 °C. Y and Th release rates are low and are similar, with elemental release rates at 700 °C higher than those at other heating temperatures. The elemental releases for Th, Y and U are broadly consistent with the complex nature of the recrystallisation process. Pb release rates increase with increasing annealing temperature. The temperature dependence of Pb release is consistent with the formation

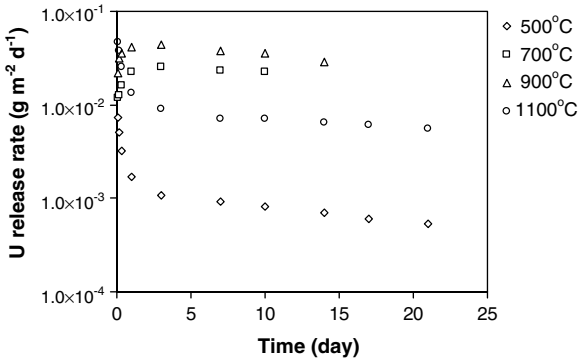

Fig. 7. U release rates for the natural brannerite annealed at different temperatures, based on BET surface areas.

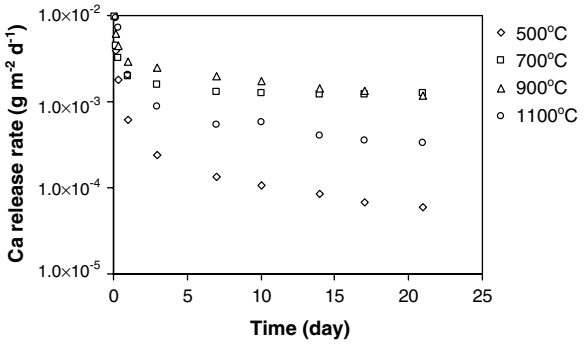

Fig. 8. Ca release rates for the natural brannerite annealed at different temperatures, based on BET surface areas.

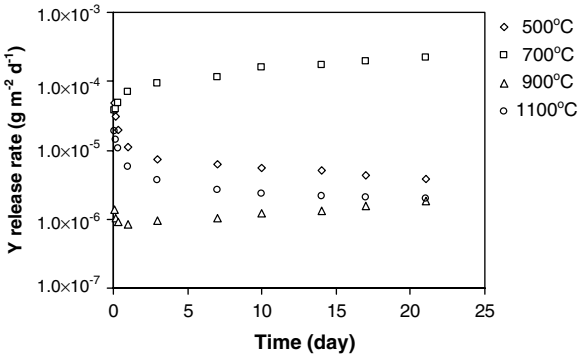

Fig. 9. Y release rates for the natural brannerite annealed at different temperatures, based on BET surface areas.

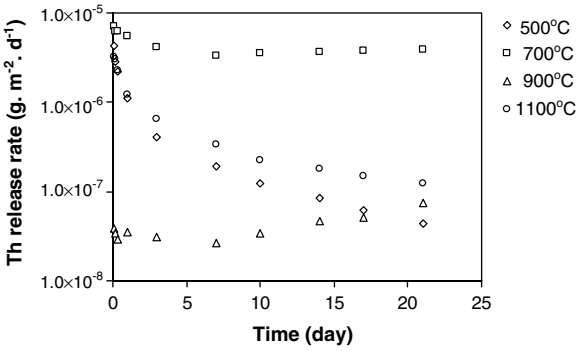

Fig. 10. Th release rates for the natural brannerite annealed at different temperatures, based on BET surface areas.

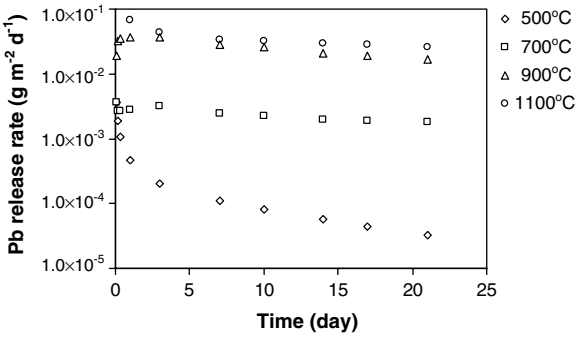

Fig. 11. Pb release rates for the natural brannerite annealed at different temperatures, based on BET surface areas.

of soluble Pb-rich glass in the triple points. Ti release rates are low, ranging from 10^{-6} to 10^{-5} g m^{-2} d^{-1} (not shown). However, the key elements present are U and Ti, so their release rates will largely control the overall dissolution rate.

3.6. The effect of radiation damage

When compared to synthetic brannerite [12], the amorphous natural brannerite (after annealing in argon at 500 °C) gives about one order of magnitude higher uranium release rate. However, compared to the fully recrystallised brannerite sample (after annealing in argon at 1100 °C), the amorphous natural brannerite gives nearly an order of magnitude lower uranium release rate, less than 10^{-3} g m^{-2} d^{-1} after 3 days. This result shows that thermal recrystallisation of the amorphous natural brannerite can further deteriorate the chemical durability, contrary to expectation that radiation damage decreases aqueous durability. However Strachan et al. [13] have shown that amorphous zirconolite does not significantly affect chemical durability. In the present case, the decrease of durability upon recrystallisation, as measured by the U release rates, might well be due to enhanced UO_{2+x} formation. We have recently found that UO_2–ThO_2 solid solution contains amounts of U^{5+} after being heated in argon at elevated temperatures and this would likely results in enhanced U dissolution.

4. Conclusions

Physical characterisation of the natural brannerite has shown only minor alteration over geological time even though radiation has rendered the structure aperiodic. The recrystallisation of amorphous natural brannerite through annealing in an argon atmosphere results in the formation of UO_2 particles among the recrystallised brannerite grains and some relatively soluble Pb-rich aluminosilicate glass films in the triple points, and this probably accounts for the higher U and Pb release rates for the recrystallised brannerite. Overall, the natural brannerite has been shown to be resistant to dissolution over geological time and the presence of this phase in ceramic formulations used for the immobilisation of actinide-rich radioactive wastes should not be detrimental to the use of these wasteforms for long-term geological disposal.

Acknowledgements

The natural brannerite sample was provided by Dr Carl A. Francis of the Harvard University Mineralogical Museum, Cambridge, Massachussetts, USA. We would like to thank E. Drabarek for BET surface area measurements.

References

[1] R.O. Ifill, A.H. Clark, W.C. Cooper, CIM Bull 82 (1989) 65.
[2] R.O. Ifill, W.C. Cooper, A.H. Clark, CIM Bull 89 (1996) 93.
[3] J.T. Szymanski, J.D. Scott, Can. Miner. 20 (1982) 271.
[4] G.R. Lumpkin, S.H.F. Leung, M. Colella, in: R.W. Smith, D.W. Shoesmith (Eds.), Mat. Res. Soc. Symp. Proceeding, vol. 608, 2000, p. 359.
[5] B.B. Ebbinghaus, R.A. VanKonynenburg, F.J. Ryerson, E.R. Vance, M.W.A. Stewart, A. Jostsons, J.S. Allender, T. Rankin, J. Congdon, Waste Management 98 (CD-ROM), Tucson, AZ, USA, 5 March 1998.
[6] E.R. Vance, J.N. Watson, M.L. Carter, R.A. Day, G.R. Lumpkin, K.P. Hart, Y. Zhang, P.J. McGlinn, M.W.A. Stewart, D.J. Cassidy, Ceramic Trans., Am Ceram. Soc. 107 (2000) 561.

[7] Y. Zhang, B.S. Thomas, G.R. Lumpkin, M. Blackford, Z. Zhang, M. Colella, Z. Aly, J. Nucl. Mater. 321 (2003) 1.
[8] J.E. Patchett, E.W. Nuffield, Can. Miner. 6 (1960) 483.
[9] V. Balek, V. Zelenák, Z. Málek, E.R. Vance, J. Subrt, in: K.P. Hart, G.R. Lumpkin (Eds.), Mat. Res. Soc. Symp. Proceeding, vol. 663, 2001, p. 347.
[10] M. Colella, G.R. Lumpkin, Z. Zhang, E.C. Buck, K.L. Smith, Phys. Chem. Miner. 32 (2005) 52.
[11] G.R. Lumpkin, K.L. Smith, M.G. Blackford, R. Giere, C.T. Williams, Micron 25 (1994) 581.
[12] Y. Zhang, K.P. Hart, W.L. Bourcier, R.A. Day, M. Colella, B. Thomas, Z. Aly, A. Jostsons, J. Nucl. Mater. 289 (2001) 254.
[13] D.M. Strachan, R.D. Scheele, E.C. Buck, J.P. Icenhower, A.E. Kozelisky, R.L. Sell, R.J. Elovich, W.C. Buchmiller, J. Nucl. Mater. 345 (2005) 109.